Differences Between Apo and Three Holo Forms of the Intestinal Fatty Acid Binding Protein Seen by Molecular Dynamics Computer Calculations

Thomas B. Woolf,*,† Alan Grossfield,† and Michael Tychko*

*Departments of Physiology and of †Biophysics and Biophysical Chemistry, Johns Hopkins University School of Medicine, Baltimore, MD 21205

ABSTRACT It is commonly believed that binding affinity can be estimated by consideration of local changes of ligand and protein. This paper discusses a set of molecular dynamics simulations of intestinal fatty acid binding protein addressing the protein's response to presence or absence of different ligands. A 5-ns simulation was performed of the protein without a ligand, and three simulations (one 5-ns and two 2-ns) were performed with different fatty acids bound. The results indicate that, although the basic protein structure is unchanged by the presence of the ligand, other properties are significantly affected by ligand binding. For example, zero-time covariance patterns between protein, bound waters, and ligand vary between the different simulations. Moreover, the interaction energies between ligand and specific residues indicate that different ligands are stabilized in different ways. In sum, the results suggest that binding thermodynamics within this system will need to be calculated not from a subset of nearby protein:ligand interactions, but will depend on a knowledge of the motions coupling together water, protein, and ligand.

INTRODUCTION

The key molecular interactions that describe ligand binding affinity are still a matter of debate. A complete theory of ligand discrimination would be able to describe the types of motions and energetic connections that define selectivity for a particular ligand within a particular system. In molecular simulations, binding calculations usually focus on a circumscribed region of the protein near the binding site. This effectively assumes that the binding affinity can be understood as a sum of local energetic interactions and that the behavior of more distant parts of the system site do not significantly affect the result (Dill, 1997).

The current paper reports on molecular dynamics calculations of the intestinal fatty acid binding protein (I-FABP). This protein is part of large gene family of cellular proteins, called lipid binding proteins or fatty acid binding proteins (FABPs), involved with lipid binding (Sacchettini and Gordon, 1993; LaLonde et al., 1994). These proteins are useful as models for understanding details of protein recognition of specific lipids (Sacchettini and Gordon, 1993; LaLonde et al., 1994). Moreover, understanding the interactions driving the binding of free fatty acids as ligands may help us explain the behavior of membrane proteins and the mechanisms of lipid transport within the cell. For these reasons, simulations are reported for the apo form (no ligand bound), and three holo forms (bound myristate, palmitate, and oleate).

The lipid binding proteins are excellent candidates for investigation by molecular dynamics simulation, for a variety of reasons. There are a number of high quality x-ray structures (Sacchettini et al., 1989, 1992; Scapin et al., 1992; Eads et al., 1993), ongoing nuclear magnetic resonance (NMR) work (Cistola et al., 1989, 1990; Hodsdon et al., 1995; Cistola and Hall, 1995; Hodsdon et al., 1996; Hodsdon and Cistola, 1997a,b; Zhang et al, 1997; Mesgarzadeh et al., 1998), and excellent binding thermodynamics studies (Richieri et al., 1992, 1994, 1995, 1996, 1998; Kirk et al., 1996; Kurian et al., 1996), all of which provide an excellent resource for comparison to simulations. In particular, binding affinity experiments have shown that the proteins are capable of discrimination of lipid type based on chain length, saturation, and headgroup type.

Examination of the different crystal structures shows a large number of ordered water molecules buried in the central cavity of all FABPs. Some but not all of these waters are displaced upon ligand binding, which suggests that their behavior should not be neglected when considering issues of binding stability and specificity. Previous simulations indicated that the diffusion constants of waters in the interiors of the muscle and adipocyte fatty acid binding proteins are significantly reduced relative to bulk (Woolf, 1998; Woolf and Tychko, 1998), indicating that this is likely to be the case for I-FABP as well. This is consistent with NMR analysis of internal waters in the M-FABP (Mesgarzadeh et al., 1998). The detailed role of internal water in determining binding affinity and selectivity thus remains to be determined. Computer calculations can help with this question by examining the energetics of the interaction between particular waters and the protein. For example, water that displays high interaction energies or highly correlated motion may play a role in binding function.

An important issue for analysis of binding affinity is the degree to which ligand binding can be considered a local phenomenon. Molecular dynamics simulations allow us to directly test this hypothesis by examining differences be-

Received for publication 19 January 1999 and in final form 4 November 1999.

Address reprint requests to Thomas B. Woolf, Department of Physiology, The Johns Hopkins University School of Medicine, 725 N. Wolfe Street, Baltimore, MD 21205. Tel.: 410-614-2643; Fax: 410-614-4436; E-mail: woolf@groucho.med.jhmi.edu.

0006-3495/00/02/608/18 $2.00

tween interaction energies and zero-time covariances in simulations of I-FABP with and without ligands. We do not attempt, in this paper, to directly compute binding affinity for the ligands. However, analysis of the interaction energies gives some indication of the enthalpic contributions to ligand binding, while covariance analysis can tell us which parts of the system are likely to be involved entropically. Although these analyses cannot directly rationalize binding affinities, it is intriguing to note the quite different patterns of interaction and zero-time covariance seen in the simulations.

METHODOLOGY

All simulations used the molecular dynamics program CHARMM (Brooks et al., 1983). The recently developed lipid-protein potential function of (Schlenkrich et al., 1996) was used for all calculations.

Simulation size and boundaries

All simulations were initiated from x-ray structures. The apo simulation was constructed using coordinates from Scapin et al. (1992), the myristate simulation used the structure from Eads et al. (1993), the palmitate simulation was from the first of four structures determined by Sacchinetti et al. (1989) and the oleate was from the structure of Sacchinetti et al. (1992).

The water droplet model was used to solvate the protein. In this approach, the protein is first surrounded by a large box of equilibrated water extending beyond the nonbonded cutoff distance of the protein. The water box is then converted into a sphere by deletion of all molecules beyond a certain distance from the system center. This varied slightly, from one system to another, but was generally near 30 Å. Waters within 2.6 Å of any protein or ligand heavy atoms were also deleted. A radial boundary potential applied to water oxygens prevents the droplet from dispersing. This potential is zero for distances under 27.5 Å from the system center, has a small (roughly -0.25 kcal/mol) minimum at 28.6 Å, and climbs quarticly thereafter. The protein was solvated by roughly 2000 TIP3 water molecules, bringing the total system size to 8500 atoms. Electrostatic interactions were shifted to zero at 12 Å, and van der Waals interactions were switched off between 10 and 12 Å.

The water droplet approach was first used in the context of an enzyme-active site (Brünger et al., 1984) and has since been used by many other groups to reduce the number of waters needed for effective solvation, and thus enable longer simulations. The choice of these boundary conditions will have an effect on the motions of the protein and especially on the side chains of the protein surface, but it is expected that the internal binding site, the internal waters, and the internal ligand (when present) will not be changed dramatically. It should be noted that the amount of water used is significantly greater than a thin shell of waters surrounding only the surface, with generally a 12-Å buffer zone of water surrounding the closest approach of protein surface to the boundary. Thus, water exchange from the outer to the inner environments is expected to be reasonable. Moreover, because all of the simulations discussed in this paper were run using the same methods, possible systematic shifts caused by the boundary conditions can most likely be neglected when comparisons are presented.

The appropriate charge state of the fatty acid ligand was determined through Poisson-Boltzman calculations (Gilson et al., 1988). The calculations suggested that the lipid headgroup should be charged while bound to I-FABP, consistent with the available experimental evidence for the system (Cistola et al., 1989). A similar calculation for the M- and A-FABP systems indicated that neutral headgroups would be more stable at pH 7 (Woolf, 1998; Woolf and Tychko, 1998). Previous simulations of the M- and A-FABP systems (a total of five) indicated that neutral headgroups were necessary to generate stable trajectories; simulations of charged fatty acids rapidly diverged from the initial structure.

Construction and equilibration

The systems were constructed by first adding hydrogens to the heavy atoms of the x-ray structures. The structures were then gently relaxed with a series of steepest descent minimizations with decreasing harmonic restraints on all heavy atoms. The system was then solvated as described above.

Each system was minimized and equilibrated in the same manner. A series of steepest descent minimizations was performed, first with the protein, x-ray water, and fatty acid atoms fixed, and then with decreasing harmonic restraints on those atoms. No restraints were placed on the bulk waters. This was followed by 2 ps of dynamics with harmonic restraints on the heavy atoms of the x-ray resolved water, protein, and fatty acid. A further equilibration period of 50 ps was used before conformations were saved. For the first 25 ps, Langevin dynamics with a frictional coupling constant of 25 ps and a temperature of 300 K was used. During the rest of equilibration, the system temperature was controlled by rescaling the velocities whenever the temperature deviated from 300 K by more than 5 K. The temperatures were checked every 2.5 ps.

Production

Trajectory production consisted of 5 ns of simulation time for two of the systems (apo and oleate) and of 2 ns simulations for the remaining two systems (palmitate and myristate). System temperature remained stable near the value of 300 K in all simulations after the equilibration procedure.

Analysis

All analysis was performed either using CHARMM or locally written programs. The analysis of dihedral changes, rms deviations, interaction energies, and covariance were all determined within CHARMM.

For purposes of analysis, the water populations of the simulations were divided at each time point into four populations. The first population was a strictly defined internal water population. The definition, though arbitrary, allowed for a consistent definition of those waters clearly found inside the binding cavity. Specifically, those waters found within 2.5 Å of obviously internal protein atoms (residues Y14 (HH, OH), D34 (OD1,OD2), E51 (OE1,OE2), S53 (HG1), Y70 (OH), T76 (OG1, HG1), Q115 (HE21), Y117 (HH), R126 (HH22)) or near the ligand were considered interior. This criterion consistently defined a set of waters that was close in number to those found in the x-ray structures.

The second set of waters was defined as those waters within hydrogen bonding distance (2.5 Å) of the protein backbone. A third set of waters was defined as those near side chains of the 61 internal amino acids. The set of 61 internal side chains was determined from the x-ray structures. The fourth set of waters was defined as the remaining waters at each time point after the other three sets had been defined. This same definition of waters was used consistently throughout the analysis to enable a fair comparison between the structures.

For purposes of analysis and comparison to the x-ray literature, the protein secondary structural elements were taken from Sacchettini et al. (1989). Beta strands: A:(residues 3–12), B:(34–43), C:(46–53), D:(55–63), E:(67–73), F:(75–85), G:(88–96), H:(100–109), I:(111–119), J:(123–131), and α-helices A-I:(13–21) and A-II:(24–33).

Analysis scripts were written in Perl to extract the populations of water near the backbone and water occupancy inside the protein. In particular, the contact frequency of a water was defined as the fraction of time during the simulation that a particular water was in contact with another group (e.g., protein location or fatty acid). The figures and tables show highlights of the analysis. More complete tables and figures are available from the authors on request.

RESULTS

Four simulations of intestinal fatty acid binding protein (I-FABP) are described. Two simulations (apo and oleate) are for 5 ns duration, and the other two (myristate and palmitate) are for 2 ns.

Simulation stability

Fig. 1 shows time series overlays of apo and oleate I-FABP with eight conformations separated by 500 ps. The results show the simulation was stable on the time scale of the molecular dynamics calculations. This suggests that the potential function, boundary conditions, and equilibration route led to a system that was well equilibrated and not one that rapidly became unstable. If the charge state of the fatty acid was chosen incorrectly, divergence from the x-ray structures would likely have occurred on this time scale (Woolf, 1998; Woolf and Tychko, 1998). Note that the two overall backbone conformations remained relatively the same throughout both simulations.

Several results are visible on comparison of the overlay series. Although the two systems do not show dramatically different overall mobilities, some differences are seen in the "lid" region defined by the two α helices and the loops between strands C:D and E:F. In particular, the two helices seem to have greater motion in the apo than the oleate run, while the loops seem to have greater mobility in the oleate simulation.

Fig. 1 also shows that the loop regions in general have greater mobility than the regions of secondary structure defined by the β sheets. This is a general trend seen in x-ray B-factors and in other molecular dynamics calculations.

Backbone dihedrals

Fig. 2 presents the observed average and r.m.s. deviations for the backbone dihedrals of all four simulations. The presentation uses positive values for the ϕ angles and negative values for the ψ angles in order to allow the full set of dihedral angles to be presented in a single figure. The average and r.m.s. are for the full length of trajectory in each case. The results further emphasize that the simulations were stable on the nanosecond time scale. The r.m.s. deviations in backbone dihedral are largest in the loop regions. This is consistent with the overlay plots (Fig. 1) and with expectations of general protein behavior. It is clear from the figure which regions are β sheet and which α helix both from the range of ϕ and ψ values as well as the smaller r.m.s. fluctuations.

The similar size of fluctuations in all four simulations suggest that the discrimination of lipid type is largely defined by changes in the internal environment of the protein cavity and not by large changes in backbone ϕ and ψ angles.

Fatty acid dihedrals

The fatty acid alkane chains did not stay in a single conformation throughout the trajectory. Instead, changes in the alkane chain dihedral angles were observed in the trajectories. The changes were not frequent enough to statistically ascertain their coupling, but it appears that correlated i:i+2 changes in the alkane chain dihedral angles were more common than i:i+1 and i:i+3 changes. This is consistent

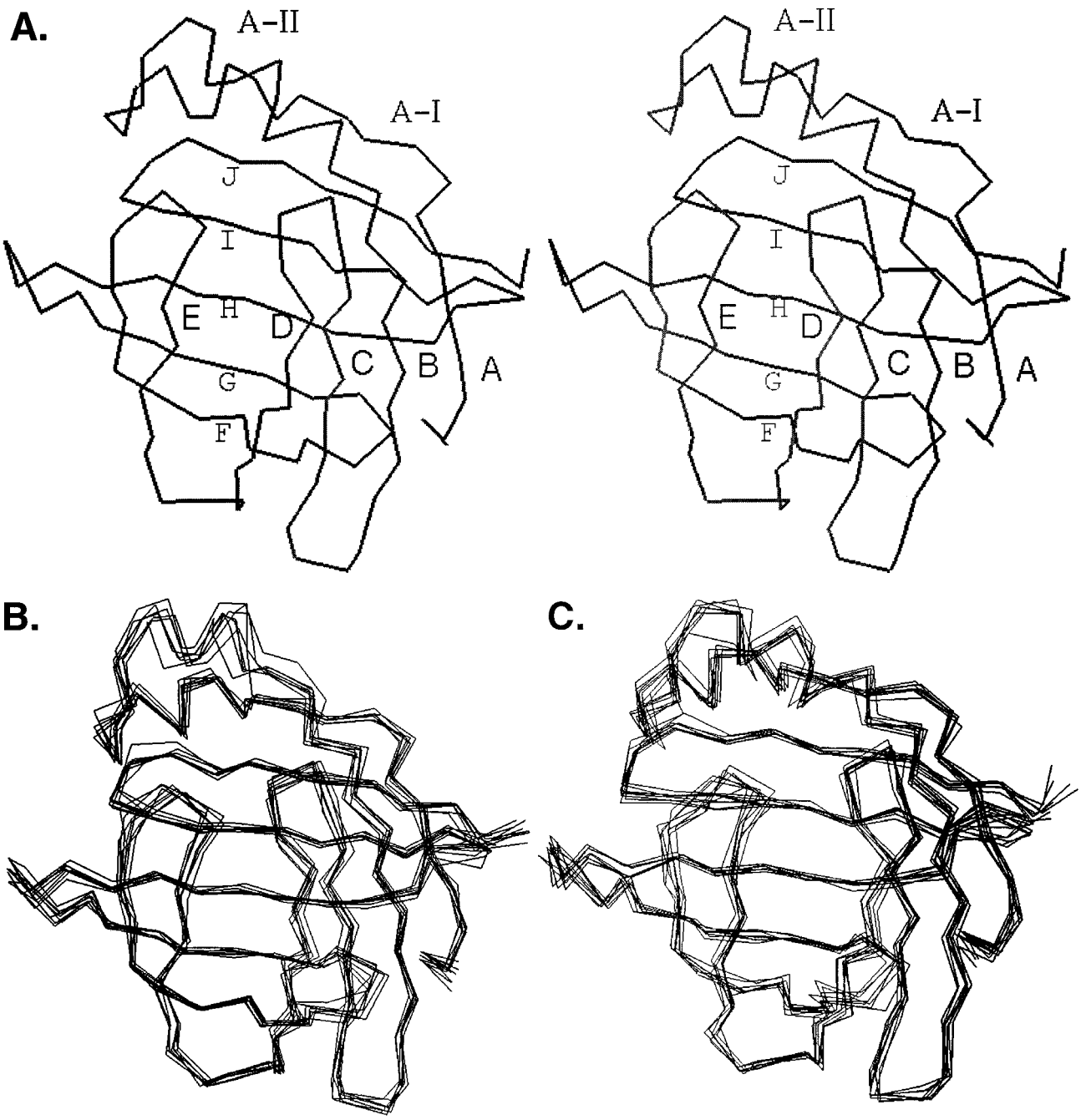

FIGURE 1 The overall fold of the intestinal fatty acid binding protein is shown as a stereo pair in A. Helvetica font is used for the five β strands, A-E, in the part of the structure facing the viewer. The five β sheets, F-J in the back part of the binding cavity, are denoted in Courier font. The two α helices are indicated as A-I and A-II. (*B* and *C*) A series of backbone snapshots from the two 5-ns trajectories. The eight conformations are separated by 500 ps in each case. *B* shows the apo form and *C* is from the oleate simulations.

with previous FABP simulations and with simulations of neat lipid bilayers (Woolf, 1998; Woolf and Tychko, 1998; Brown et al., 1995).

The time series of these dihedrals are presented in Fig. 3. The ordering is from the headgroup (lowest) to the terminal methyl group (highest). The vertical displacement between time series is arbitrary (360 degrees) and allows the full set of timeseries to be presented on a single graph. Notice the longer time scale for the oleate calculations and the presence of the single double bond (reflected in the dihedral with no changes).

Table 1 presents the statistics for total number of observed dihedral changes and the numbers of i:i+1, i:i+2, i:i+3 changes that both occurred within a window of 3.0 ps.

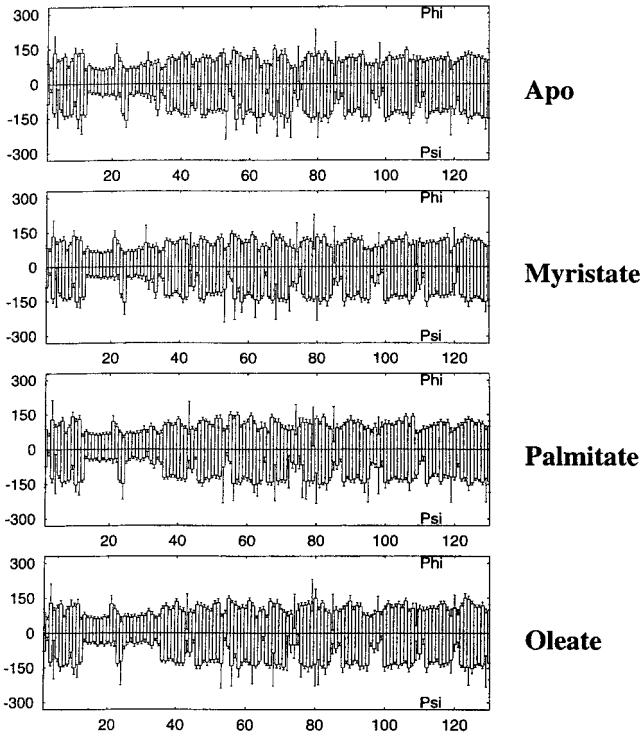

FIGURE 2 The ϕ-ψ values of the protein backbone presented as average and r.m.s. deviations. The ϕ values are presented along the positive axis, and the ψ values are along the negative axis.

This window size was determined to be optimal in calculations of Brown et al. (1995).

Water behavior

Many waters entered and exited the protein cavity during the course of the simulations. The properties of the water varied widely depending on the effective binding site or sites that it encountered within the protein interior. Unsurprisingly, those waters that had the strongest interactions within the protein had the slowest effective diffusion times and exchanged least frequently with other waters. Waters that had a relatively weaker binding within the cavity tended to move more during the simulation and tended to exchange with other waters more readily.

To quantify the water behavior in some detail, an attempt was made to identify all the possible sites for water hydrogen bonding within the interior of the protein. Especially interesting was water that had interactions with both the ligand and other waters or parts of the protein. Given the list of sites, the trajectories were then assayed for the relative occupancy of each location and for the relative strength of the interactions by determining the relative interaction energy between water occupying the site and the surroundings. These results are presented in Table 2, where the ten waters most frequently found in the cavity interior are described, and in Table 3 for the ten most frequent sites defined by the protein backbone.

Several interesting things were noted in the analysis. First, all four simulations had many interior waters that exchanged positions with outside waters during the trajectory. This implies a highly dynamic set of waters not confined within the interior cavity for lifetimes on the order of the simulation time. Table 3 can be used as a suggestion for water exchange lifetimes. For example, note that W82 (part of the hydrogen bonding network with the carboxylate headgroup and R106) had a water present for long lifetimes in all four of the simulations.

Interaction energy: fatty acid

To initiate an understanding of the binding thermodynamics, interaction energies were calculated between the fatty acid and the surrounding matter. In particular, the question was asked: what are the main contributions to the interaction energy? The resulting trajectory-averaged interaction gives an interaction enthalpy which reflects only part of the full thermodynamics of binding. Despite the incomplete nature of this information for binding affinity, the results can still suggest insight into the molecular details of binding. Fig. 4 shows the contributions to the interaction energy for the three holo systems. The first part of the figure shows the strength of interaction for the headgroup of the fatty acid interacting with the rest of the system versus the tail of the fatty acid interacting with the rest of the system. This should be contrasted with our previous simulations of the human muscle and adipocyte FABPs containing an uncharged ligand (Woolf, 1998; Woolf and Tychko, 1998). The charged fatty acids in the current simulations create a significantly larger net interaction between the headgroup and its surroundings. The interaction energy was further analyzed by considering the contributions from individual methylene groups along the length of the fatty acid. The results (not shown) emphasized the presence of variability along the alkane chain length. That is, the binding cavity is a highly heterogeneous binding environment, with different fatty acid interactions depending on location in the cavity.

It is also interesting to note that the headgroup interaction for each of the simulations is different, whereas the tail interaction is similar. In particular, the interactions with the ligand headgroup were strongest in the myristate simulation. Moreover, this simulation also had the broadest distribution of interactions.

Interaction energy: amino acid

The fatty acid:protein interactions can be further analyzed by examining the interactions made by individual amino acids. This is shown in Fig. 5, where the ligand interaction with each amino acid in the holo simulations is shown.

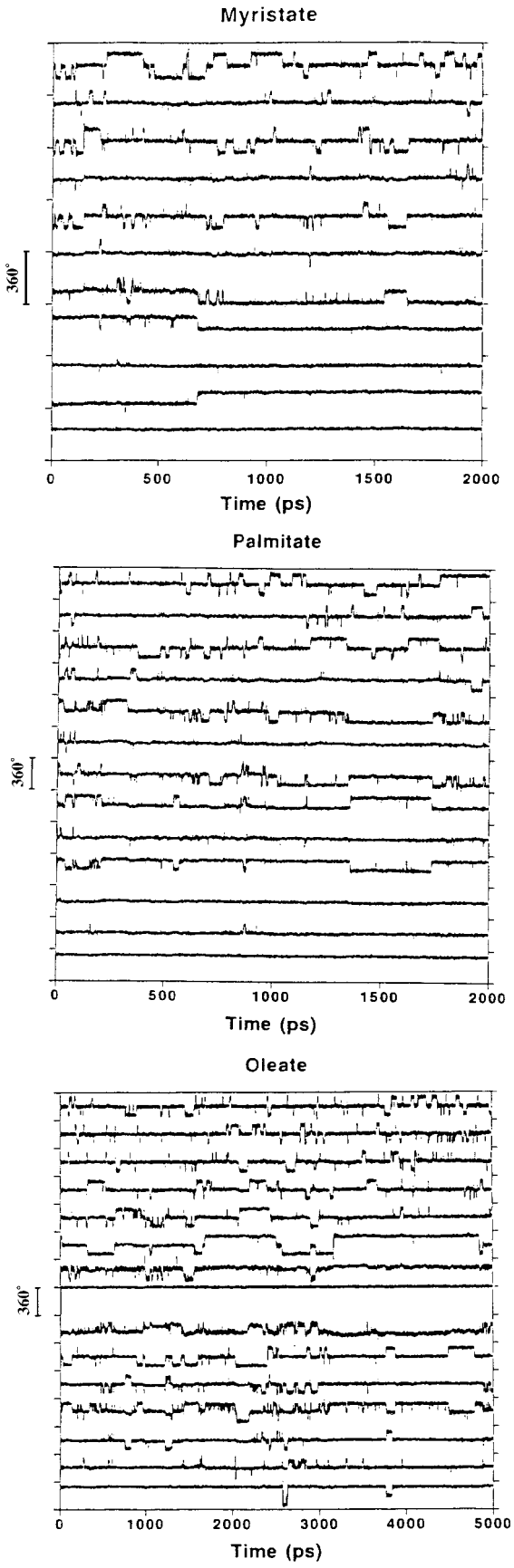

These results can be divided into side chain and backbone contributions. This is interesting, since the Kleinfeld group has analyzed the behavior of a series of alanine mutants (Richieri et al., 1997, 1998). Assuming everything else remained constant, these mutations would involve changes only with the mutated side chain, leaving backbone interactions unchanged.

The figure shows intriguing differences in the interaction energy between the different side chains and the fatty acid. Particularly interesting is the observation that the main chain contributions tend to be relatively small, whereas the side chain contributions can vary over a larger range. Notice also that each fatty acid contributes differently to the interaction energies. This may be related to the ability of I-FABP to discriminate between fatty acids on the basis of chain length and saturation state (Richieri et al., 1995).

Interaction energy: comparison with apo

The two panels of Fig. 6 show the interaction of the internal amino acids defining the binding site with either all other side chains or the strictly defined internal water. The interaction energies were determined for the full amino acid and thus include both main chain and side chain contributions. A major focus of this analysis was the differences in interaction energy for this subset of amino acid residues across all four simulations. Thus, the key to the left of the figure indicates the simulation from which the interaction energy was calculated. Interactions were also calculated for this same set of amino acids with the other three water categories described above, and with the rest of the protein's backbone. The results to be discussed will include both analysis of the two sets of calculations shown and the four sets of calculations not shown.

In looking at the figure, note that the vertical interaction energy scale changes from one panel to another. For example, the charged amino acids have a scale that is much larger than the polar amino acids (-80 to 40 versus -10 to 5 kcal/mol on the lower panel).

Several aspects were revealed by the analysis. First, the internal waters interact strongly with a subset of amino acids. This suggests restricted diffusion and a type of binding site for waters. Specifically, Y14, Y117, D34, E51, G31, L72, S53, T76, and Q115 are the strongest interacting residues with strictly defined internal waters. This behavior is relatively invariant across the four simulations. Only G31 and Q115 had significant differences in their interaction energies between the four simulations, and only G31 varied

FIGURE 3 Time series for the dihedral angles along the fatty acid chain from the three holo simulations. The curves are shifted by 360 degrees along the vertical axis for clarity. The lowest time series is for the dihedral from the headgroup, and the top time series is for the terminal dihedral along the fatty acid.

TABLE 1A Dihedral transitions in myristate within the I-LBP

Dihedral number	Total number of transitions	Number of i:i + 1 transitions	Number of i:i + 2 transitions	Number of i:i + 3 transitions	Number of i:i + 4 transitions
3	0	0	0	0	0
4	2	0	0	0	0
5	0	0	0	0	0
6	0	0	0	0	0
7	17	0	6	0	1
8	1	0	0	0	0
9	30	0	9	0	3
10	1	0	1	1	0
11	22	1	4	0	1
12	4	2	1	0	0
13	16	1	1	1	3

Dihedral number 3 is defined by the C1-C2-C3-C4 atoms. Dihedral number 13 is defined by the C11-C12-C13-C14 atoms. Dihedral number 15 (1B) is defined by the C13-C14-C15-C16 atoms. Dihedral number 17 is defined by the C15-C16-C17-C18 atoms. Note that the number of paired transitions does not sum to the total number of transitions because more than a pair of transitions may occur within a single window. The window size was 3.0 ps (from Table II of Brown et al., 1995).

TABLE 1B Dihedral transitions in palmitate within the I-LBP

Dihedral number	Total number of transitions	Number of i:i + 1 transitions	Number of i:i + 2 transitions	Number of i:i + 3 transitions	Number of i:i + 4 transitions
3	0	0	0	0	0
4	6	0	3	0	2
5	0	0	0	0	0
6	22	2	10	5	1
7	10	2	5	0	1
8	21	7	9	2	3
9	52	8	13	6	6
10	7	3	4	1	3
11	53	3	15	2	6
12	17	4	3	3	1
13	44	3	13	1	6
14	17	3	1	0	2
15	39	3	6	2	5

TABLE 1C Dihedral transitions within oleate in the I-LBP

Dihedral number	Total number of transitions	Number of i:i + 1 transitions	Number of i:i + 2 transitions	Number of i:i + 3 transitions	Number of i:i + 4 transitions
3	5	0	3	0	1
4	26	1	13	3	3
5	13	3	7	2	1
6	59	12	24	9	0
7	33	12	16	3	3
8	26	6	11	4	4
9	34	4	15	9	2
10	0	0	0	0	0
11	36	2	12	5	3
12	12	4	6	1	2
13	35	6	16	5	8
14	24	7	11	5	0
15	27	6	18	1	1
16	41	13	5	5	1
17	51	10	11	2	7

between holo simulations. In this case it was a smaller interaction energy for the myristate than for apo, palmitate, or oleate.

The backbone-defined waters in general saw significant interactions with a larger set of internal residues. The amino acid residues that had been interacting strongly with the strictly defined internal waters did not interact as strongly with the backbone waters. This was especially true for Y117 and Q115. It is interesting that G31 had stronger interactions with backbone waters for apo and myristate. This suggests a degree of constant amino acid:water interaction energy for this particular amino acid.

The side chain waters (again distinct from the first two water populations) show more variability among the four simulations than the other two water populations. The nine strongly interacting sites for the strictly defined internal water see weak interactions with the water defined by side chains.

The remaining water (not defined by the other three) still contributes significantly to the interaction energy. This is especially true for sites near the dividing point between the inside and outside of the I-FABP. For example, the K27 site has an especially strong interaction with water and much weaker interactions with water in the other three populations. It is interesting to note that only Y14 of the nine strongly interacting sites of the figure shows much interaction energy with the remaining waters. Comparing across the full set of interaction energies, it was found that some residues (F2, W6, F17, F47, F62, F93, F128, R56, R106, R126, A104, L89, L102, L113, and M18) do not, on average, interact with any of the waters. Examination of the interactions of these same amino acids with other main chain and side chain atoms helps to rationalize the lack of observed water interactions. The remaining interactions are largely direct interactions with the fatty acid ligand (i.e., R106 with the headgroup). For example, W6, F17, F47, F62, F93, F128, A104, L89, L102, L113, and M18 have strong interactions with the protein backbone. Additionally, R56, R106, R126, L89, L102, and L113 have strong interactions with the side chains.

This analysis suggests that there are differences in the manner of interaction between the same amino acid residues in each system. That is, the presence or absence of a specific ligand leads to changes in the average interaction energy between each of the amino acids and their environment.

Covariance analysis: protein

The motional coupling between protein elements of the systems were analyzed with a zero-time covariance plot (not shown). The results showed that some regions of the protein are tightly coupled to other regions of the protein. Some of

TABLE 2A Ten frequent waters in Apo I-FABP (sorted by contact frequency)

Water number	Frequency	Contacts to water	Contacts to backbone	Contacts to inside sidechains	Contacts to outside sidechains
1	0.92	2.51	0.25	3.38	0.00
2	0.53	4.47	0.14	1.81	0.01
3	0.43	3.56	0.09	2.45	0.00
4	0.39	4.06	0.08	2.10	0.01
5	0.38	4.86	0.13	1.53	0.02
6	0.32	2.62	0.16	2.75	0.00
7	0.32	3.30	0.14	2.22	0.02
8	0.31	4.62	0.05	1.32	0.09
9	0.26	5.01	0.04	1.18	0.11
10	0.24	4.61	0.17	1.14	0.10

TABLE 2B Ten frequent waters in myristate I-FABP (sorted by contact frequency)

Water number	Frequency	Contacts to water	Contacts to backbone	Contacts to inside sidechains	Contacts to outside sidechains	Contacts to myristate
1	0.75	3.80	0.20	2.01	0.04	0.00
2	0.67	3.18	0.01	2.15	0.00	0.76
3	0.64	2.92	0.03	1.65	0.00	1.02
4	0.59	2.31	0.00	2.12	0.00	1.59
5	0.47	4.34	0.08	1.64	0.02	0.37
6	0.45	3.75	0.17	1.75	0.00	0.70
7	0.39	4.22	0.01	1.73	0.00	0.38
8	0.30	3.70	0.63	1.75	0.18	0.00
9	0.30	4.68	0.09	1.12	0.02	0.07
10	0.28	4.50	0.17	1.32	0.01	0.00

TABLE 2C Ten frequent waters in palmitate I-FABP (sorted by contact frequency)

Water number	Frequency	Contacts to water	Contacts to backbone	Contacts to inside sidechains	Contacts to outside sidechains	Contacts to palmitate
1	0.96	2.60	0.00	2.96	0.00	0.02
2	0.91	2.37	0.00	2.34	0.00	0.92
3	0.86	3.02	0.00	2.16	0.00	1.29
4	0.79	2.52	0.06	2.46	0.00	0.59
5	0.76	1.99	0.70	2.71	0.02	0.16
6	0.73	3.17	0.00	2.56	0.00	0.81
7	0.69	3.42	0.00	2.43	0.00	0.67
8	0.66	2.31	0.38	2.16	0.00	0.58
9	0.37	4.30	0.17	1.14	0.05	0.21
10	0.23	2.08	1.08	2.48	0.17	0.00

TABLE 2D Ten frequent waters in oleate I-FABP (sorted by contact frequency)

Water number	Frequency	Contacts to water	Contacts to backbone	Contacts to inside sidechains	Contacts to outside sidechains	Contacts to oleate
1	0.96	1.10	1.00	3.52	0.00	0.17
2	0.94	2.82	0.00	2.62	0.00	0.12
3	0.83	2.68	0.01	2.75	0.00	0.19
4	0.80	2.99	0.02	2.14	0.00	1.19
5	0.69	3.59	0.00	1.98	0.00	0.32
6	0.64	3.42	0.07	1.95	0.01	0.74
7	0.63	3.40	0.09	2.03	0.00	0.55
8	0.56	3.48	1.43	1.55	0.06	0.00
9	0.52	3.26	0.20	1.83	0.00	0.44
10	0.39	4.00	0.13	1.18	0.06	0.42

TABLE 3A High occupancy water:backbone hydrogen bonding apo I-FABP

Residue	Number of contacts	Average lifetime	Variation in lifetime	Percentage of time occupied
2	463	9.76	8.65	0.90
5	371	12.33	11.39	0.92
11	699	6.45	5.17	0.90
25	476	9.53	8.15	0.91
45	704	6.66	6.01	0.94
57	664	7.10	5.83	0.94
63	645	7.02	6.44	0.91
82	8	624.12	404.91	1.00
84	173	28.17	23.17	0.97
87	877	5.67	5.72	0.99
101	648	6.95	6.26	0.90
108	230	19.88	20.54	0.92
111	645	6.98	7.09	0.90
121	1304	3.46	2.67	0.90
130	396	12.17	13.48	0.96

TABLE 3B High occupancy water:backbone hydrogen bonding myristate:I-FABP

Residue	Number of contacts	Average lifetime	Variation in lifetime	Percentage of time occupied
5	110	13.13	13.24	0.96
11	225	6.11	4.80	0.92
13	339	4.22	3.55	0.95
25	154	8.75	7.98	0.90
42	115	12.14	10.66	0.93
45	317	4.79	4.49	1.0
57	213	6.47	5.28	0.92
63	102	13.68	12.58	0.93
71	187	7.28	5.99	0.91
77	187	7.75	8.33	0.97
82	4	374.25	334.38	1.00
84	55	26.62	20.67	0.98
87	250	6.14	6.47	1.0
88	86	15.78	12.17	0.91
101	197	7.01	6.52	0.92
108	73	20.16	19.55	0.98
130	99	14.39	15.18	0.95

TABLE 3C High occupancy water:backbone hydrogen bonding palmitate I-FABP

Residue	Number of contacts	Average lifetime	Variation in lifetime	Percentage of time occupied
2	183	9.87	9.10	0.90
5	268	6.92	7.27	0.93
11	270	6.76	5.38	0.91
13	345	5.37	4.81	0.93
45	585	3.56	2.98	1.00
46	147	12.48	10.99	0.92
63	197	9.27	9.13	0.91
82	10	199.10	140.70	1.00
87	497	4.09	3.74	1.00
88	142	12.63	9.70	0.90
101	300	5.99	5.40	0.90
108	116	16.18	15.88	0.94
110	743	2.48	1.68	0.92
111	264	6.83	5.12	0.90
123	319	5.64	4.93	0.90
130	243	7.62	7.14	0.93

TABLE 3D High occupancy water:backbone hydrogen bonding oleate:I-FABP

Residue	Number of contacts	Average lifetime	Variation in lifetime	Percentage of time occupied
5	764	6.10	5.75	0.93
11	626	7.40	5.99	0.93
13	993	4.79	4.06	0.95
45	1252	4.15	3.61	1.00
57	696	6.67	5.47	0.93
63	361	12.95	12.03	0.94
77	335	14.43	14.99	0.97
84	175	27.82	23.11	0.97
87	708	7.04	7.93	1.00
101	680	6.60	5.68	0.90
108	253	19.32	18.56	0.98
121	275	17.73	19.65	0.97
130	590	7.72	7.55	0.91

these correlations are present in all simulations; for example, residues within a given secondary structure element tend to move in a correlated manner, as expected. However, other regions are not exactly the same across all four simulations. In particular, the apo simulation's covariances differed from the three simulations with ligands present. This suggests that certain types of motion available to the protein are controlled by the presence or absence of the ligand.

For example, the two α helical regions (α-I from 13 to 21 and α-II from 24 to 33) have a striking degree of difference between the three holo runs as well as the apo. The helices have both positively and negatively correlated motions with the rest of the protein. In the apo form the coupling is relatively weak, whereas in the three holo forms it is stronger. For example, the myristate has α-II coupled first negatively, then two positively coupled regions and then once more negatively coupled. For oleate, α-I is more tightly interacting and the pattern of where it is negatively or positively coupled is different. Lastly, for palmitate, the two helices are both coupled into the motion of the rest of the protein, and they are coupled in roughly (though not identically) the same way; i.e., both positive or both negative to the rest of the protein. It is interesting to speculate that these changes in motional coupling depending on lipid binding indicate a gating function for these helices.

In contrast, the β sheet regions of the protein are far less strongly coupled into the motion of the rest of the protein. In all simulations, their local covariance stands out as a series of bands extending diagonally from the center diagonal. It is interesting to note that the apo form is again more weakly coupled than the three holo forms, and that the palmitate system is again the most tightly coupled. In par-

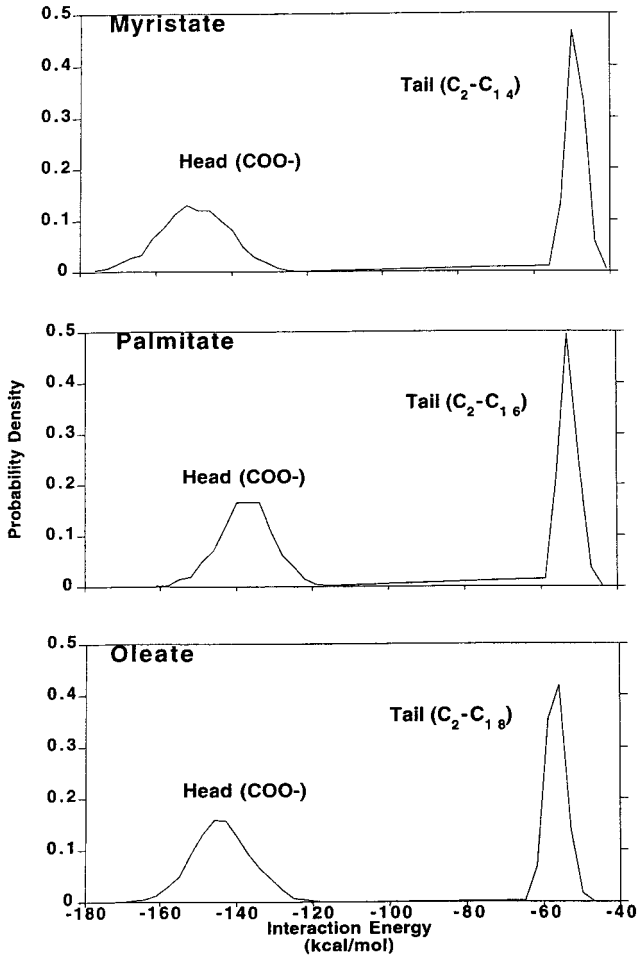

FIGURE 4 The interaction energy between protein and the bound ligand. The division is between the head and tail of the fatty acid.

ticular, a bit more anti-correlated motion is observed than in the other two holo trajectories.

Additional insight into the protein motion is seen with Fig. 7 where the coupling between interior waters and the protein is presented. Each row contains the covariance for a single water molecule with the protein α-carbons, calculated over the entire trajectory. Positively correlated motion is emphasized by coloring the square black, and negatively correlated motion is shown with a white square. Again, there are differences between the apo and the holo forms. The results are intriguing in suggesting that the presence or absence of ligand has an impact on the types of coupled motions that are present between protein and water. For example, the apo form has the weakest degree of coupling with water. Some degree of correlated motion is seen for the second α helix and β strands E and F. The myristate simulation suggests a large degree of coupling between the second α-helix and water that, although present, is not as strong in the other two holo simulations. β strand E is coupled more strongly for the palmitate and the oleate trajectories than for the myristate.

Covariance analysis: fatty acid

Insight into the possible importance of particular residues in the binding of fatty acids is shown in Fig. 8. This presents the zero-time covariance between individual amino acids and the heavy atoms of the fatty acid ligand. The results show that each of the simulations has a different type of motional coupling between the fatty acid and the protein. This is most clearly seen by a comparison of the myristate and the oleate, where the pattern is clearly different between the two systems. For example, the C strand is positively coupled with the palmitate headgroup but weakly coupled in the oleate and myristate calculations. The three simulations all suggest that the headgroup and tail covariances are anticorrelated with those for the middle of the fatty acid. For example, the palmitate strand C is positively correlated with the ligand headgroup and terminal region and negatively correlated with the midsection. It is interesting to note that the F strand is negatively correlated with the ligand in the oleate simulations and has relatively small correlations in the myristate and none in the palmitate calculations.

These patterns are different from those that were determined from simulations of the human muscle and adipocyte FABPs in our previous work (Woolf, 1998; Woolf and Tychko, 1998). This further suggests that the presence of a charged fatty acid ligand in the interior cavity, along with the sequence changes between the FABPs, leads to quite different types of motional coupling between elements of the system.

Strong coupling between the water and the ligand was observed in all three holo simulations in Fig. 8. The water selected was the most commonly found 40 waters in the strictly defined internal set for each simulation; the top ten of these are shown in Table 2. These results showed that the water plays an important role in the types of motion that can be assumed by the ligand. Separation of the covariance into head, tail, and mid-lipid behavior persists in these plots. This is especially obvious in the myristate covariance where strong divisions are seen. It is also interesting that in the oleate simulation, each water seems to correlate with longer stretches of the fatty acid chain than in the other simulations.

Comparison to NMR data

The present results can be compared with recent NMR experiments on the I-FABP system (Hodsdon and Cistola, 1997b). Specifically, the results can be compared to order parameters calculated with the Lipari-Szabo formalism (Lipari and Szabo, 1982). It should be noted that two other groups performing NMR relaxation analysis on this system report a different set of order parameters (Lucke et al., 1997; Zhu et al., 1997). This may be due to differences in the fitting of the order parameters to experimental data or to differences in experimental design and data collection.

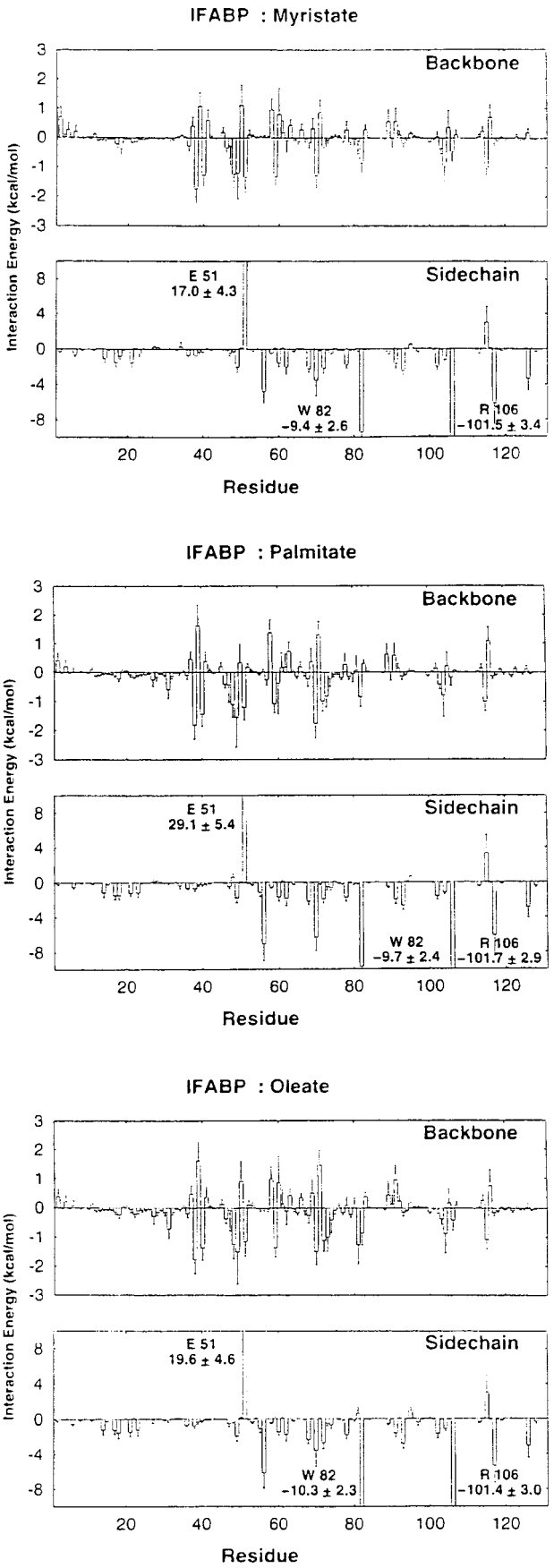

Fig. 9 shows a comparison between experimental order parameters and those calculated from the trajectories. The experimental order parameters are presented as downward deflections with a darker fill pattern. The upward deflections are from the calculated trajectories. Presented in this way, a strong match would show a symmetry about the x axis.

The results are disappointing, as there is no statistical correlation between the experimental and calculated data sets. This may be due to differences in the interpretation of the Lipari-Szabo parameters. Alternatively, the differences could be due to the assumption of an isotropic diffusion constant for the protein, which recent work with ubiquitin (Tjandra et al., 1995) suggests may not always be appropriate. Adequate sampling in the simulations may also be an issue: both trajectories were analyzed to the 2-ns time length of the palmitate run. Recent work from our group (Wrabl et al., 1998) suggests that convergence of the order parameters may take longer than 1 to 2 ns.

DISCUSSION

I-FABP is a particularly important choice for simulation because several groups have contributed to determining the structure, the binding thermodynamics, and the folding behavior (Richieri et al., 1998, 1994, 1995; Sacchettini et al., 1989, 1992; Eads et al., 1993; Scapin et al., 1992; Hodsdon et al., 1995; Cistola and Hall, 1995; Hodsdon et al., 1996; Hodsdon and Cistola, 1997a,b; Zhang et al., 1997; Frieden et al., 1995; Kim et al., 1996). The simulations cannot, at this stage, comment directly on either the molecular details of binding or folding, but insights from the simulations may suggest further interpretation of these experiments.

It is interesting to comment, at this point, on why the direct determination of binding affinity is a difficult calculation from the current simulations. If the binding affinity results could be readily interpreted in an interaction energy framework, then linear response-relative free energy methods would give a reasonable comparison with experiment, without the need to apply specialized free energy methods (Lee et al., 1992; Åqvist et al., 1994). However, such a direct calculation with the current trajectories and a companion set for the ligands alone in water did not give good agreement (data not shown). There could be several reasons for this. One strong possibility is that the behavior of water in the systems leads to a strong contribution to binding affinity that needs to be calculated with other methods. For example, the chemical potential of the water may vary with location and ligand type (as inferred from the present cal-

FIGURE 5 A breakdown of the interaction energy between individual amino acids of the protein and the fatty acid ligand. The plots present the contributions from the main chain and the side chains as separate graphs.

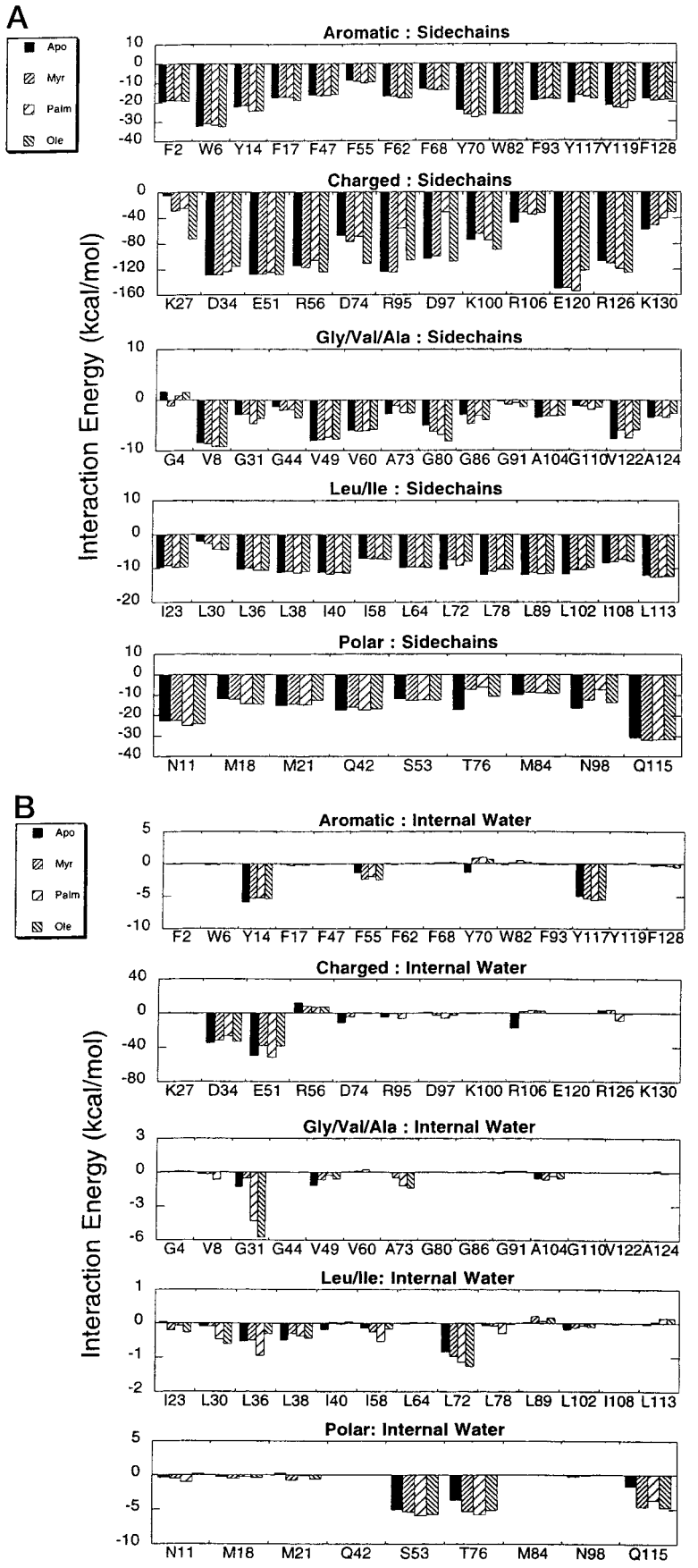

FIGURE 6 A comparison of the interaction energies between the 61 internal amino acid residues and their surroundings. The figure presents this as a function of the environment of protein side chains and of strictly internal waters. Four other similar plots to other water sets and the protein backbone are described in the text.

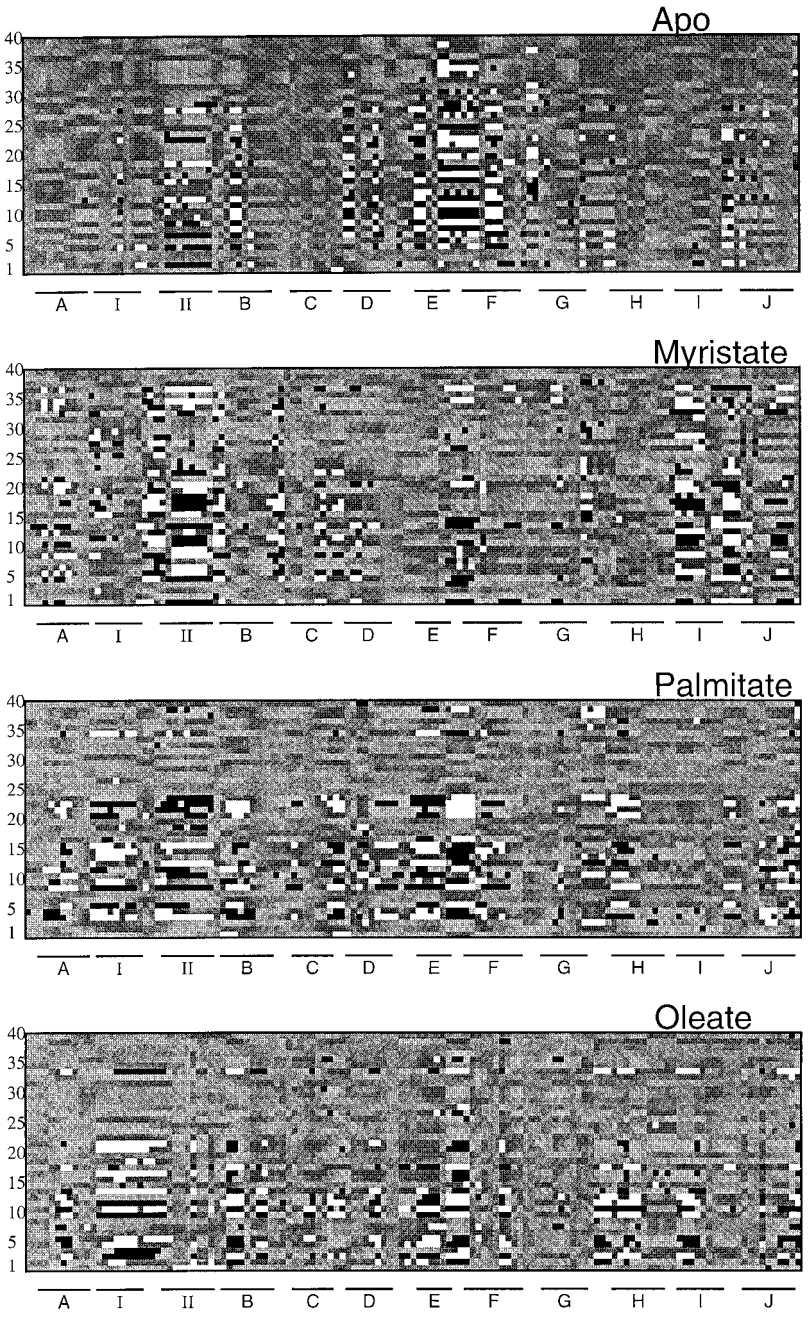

FIGURE 7 Water:protein zero time covariance. To emphasize the correlated or anti-correlated motion, the figure colors a square black if the correlated motion was greater, on average, than 0.3 and white if the anti-correlated motion was less, on average, than −0.3 The rest of the gray scale was determined with values from −0.3 to 0.3 being mapped linearly into the range 0.65 (closer to the value of white, 1) to 0.35 (closer to the value of black, 0).

culations). With water exchange present during the binding process and thus contributing to the binding thermodynamics, the problem becomes more complex than simply considering the relative contributions of van der Waals and electrostatic terms from the protein to a small set of conformations of the ligand. Another way of emphasizing this point is that the simulations may not have converged on the thermodynamic time scale where many water transitions would have converged. On the time scale of the current simulations, not enough exchange and motion of the water could present itself as a failure of linear response methods to give reasonable results.

It should again be emphasized that the direct interpretation of the differences in relative interaction energies and zero-time covariance within the context of binding affinity is not possible with the current data set. Thus, for example, the relatively large energies seen for charged and polar groups need to be be seen within the context of a thermodynamic cycle where the relevant quantity, the change upon binding, may be much smaller. Only by a set of relative free energy computations and a component breakdown of contributions could a clearer understanding of some of the differences seen in the trajectories be related to binding affinity directly.

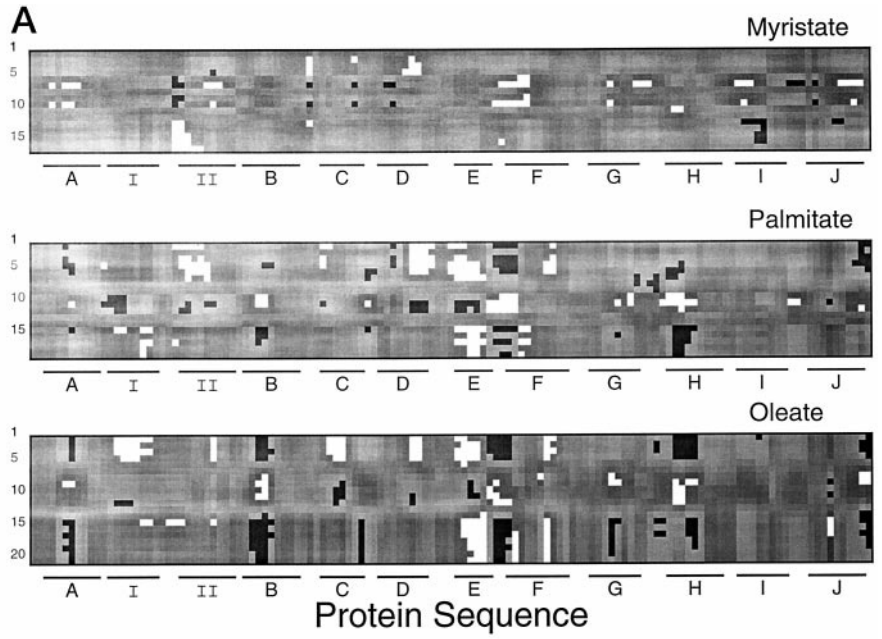

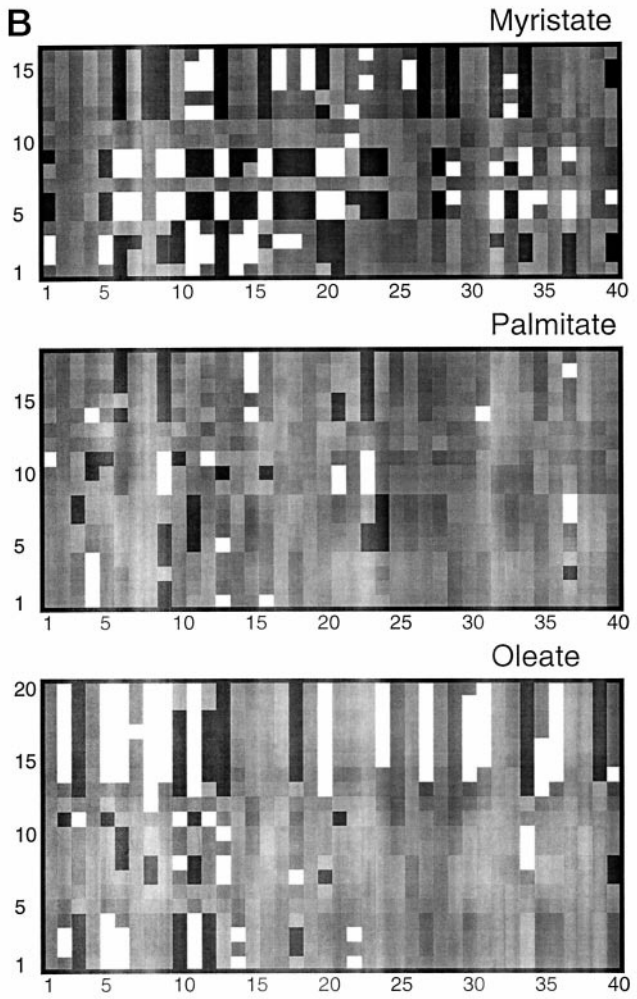

FIGURE 8 Zero-time covariance of protein and fatty acid. The vertical scale is for heavy atoms of the ligands; the horizontal scale is by heavy atoms of the protein. (*B*) A similar plot for fatty acid and water. The most common strictly defined internal 40 waters were used for the analysis.

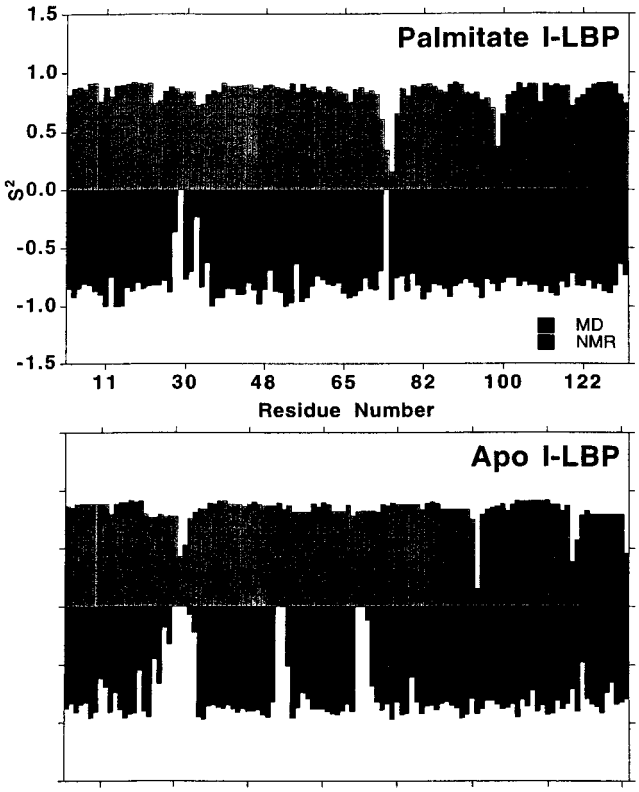

FIGURE 9 The order parameters calculated from the trajectories and their comparison to recent NMR experiment. (*A*) is for the holo comparison, (*B*) for the apo.

Further discussion of the present calculations is now first focused on particular amino acid types that have been suggested to be particularly interesting through the experimental literature. This is followed by discussion of water properties.

Tryptophan residues

The Trp residues have been used to monitor the unfolding state of the I-FABP system (Frieden et al., 1995) and for time-resolved fluorescence studies (Frolov and Schroeder, 1997). Thus, there is interest in the amount of motion and conformational change seen during the simulation. The two tryptophan residues are within different environments inside the internal cavity of the protein. W82 is within the β-F strand and the side chain has contacts with the ligand near the headgroup. In contrast, W6 is located within the first β-strand and is not in direct contact with the ligand. This is reflected in the interaction energies seen in Fig. 5, where the side chain interactions with the ligand from W82 are -10.3, -9.7, and -9.4 kcal/mol in oleate, palmitate, and myristate, respectively. The direct interactions from W6 are much smaller. Further analysis can be partially seen in Fig. 6 and in our four other analysis plots (not shown), where the different interaction energies are each compared for W6 and W82. For example, neither Trp interacts strongly with the strictly defined internal water population (Fig. 6). W82 interacts moderately with the population of waters defined by the backbone, and the interaction is independent of presence or absence of ligand (not shown). In contrast, W6 does not interact with the backbone waters. The waters defined by the internal side chains show a distinction between the W82 interactions in the apo versus the holo states (not shown). The apo interaction is among the strongest of the aromatic interactions with this population of waters. W6, for the same population, shows a very slight unfavorable interaction energy that varies with lipid type as well as between apo and holo forms. The external water population has little interaction with W6 and a stronger interaction with the apo than holo forms for W82 (not shown). The protein interactions, from the backbone, are the strongest for W6 of all aromatic interactions (not shown). The W82 interactions to the rest of the protein backbone show some change with ligand type and apo versus holo. In contrast, the interactions between both W6 and W82 to the rest of the protein side chains shows no significant change between apo/holo/ligand type (in Fig. 6). Again the W6 interaction with the protein is stronger than the W82 interaction.

The covariance analysis shows further differences between the two Trp residues. For example, the protein:protein covariance suggests that W82 in the apo form has relatively strong positive coupling to the rest of the protein through 22 sites with a covariance value greater than 0.2. For W82, negative coupling to the rest of the protein is seen at 14 sites with a value less than -0.2. In contrast, W6 shows no strong negative coupling and strong positive coupling to only eight sites. The covariance to water shown in Fig. 7 also suggests a much weaker coupling for W6 to the most common internal waters relative to the W82 coupling. Also of note were the differences in covariance between the two Trp and the fatty acids shown in Fig. 8. The W6 coupling was strongest to the myristate and showed mainly anticorrelated coupling in that case. The W82 was strongest to the oleate and showed mainly correlated motions. This difference in covariance behavior is further emphasized by analysis of the hydrogen bonding patterns for the ring hydrogen in W6 and W82. Fig. 10 shows that the ring hydrogen had a strong hydrogen bond to the oleate throughout the holo simulation, whereas the apo simulation had a set of six waters and the side chain oxygen of Tyr-70 that provided a hydrogen bonding partner.

Finally, it is interesting to note that neither Trp had dihedral changes along either χ-1 or χ-2. The average and deviations about those averages showed only minor changes in the apo/holo runs.

Phe55

Phe55 has been suggested to regulate the length of the protein in response to the lipid (Sacchettini et al., 1989).

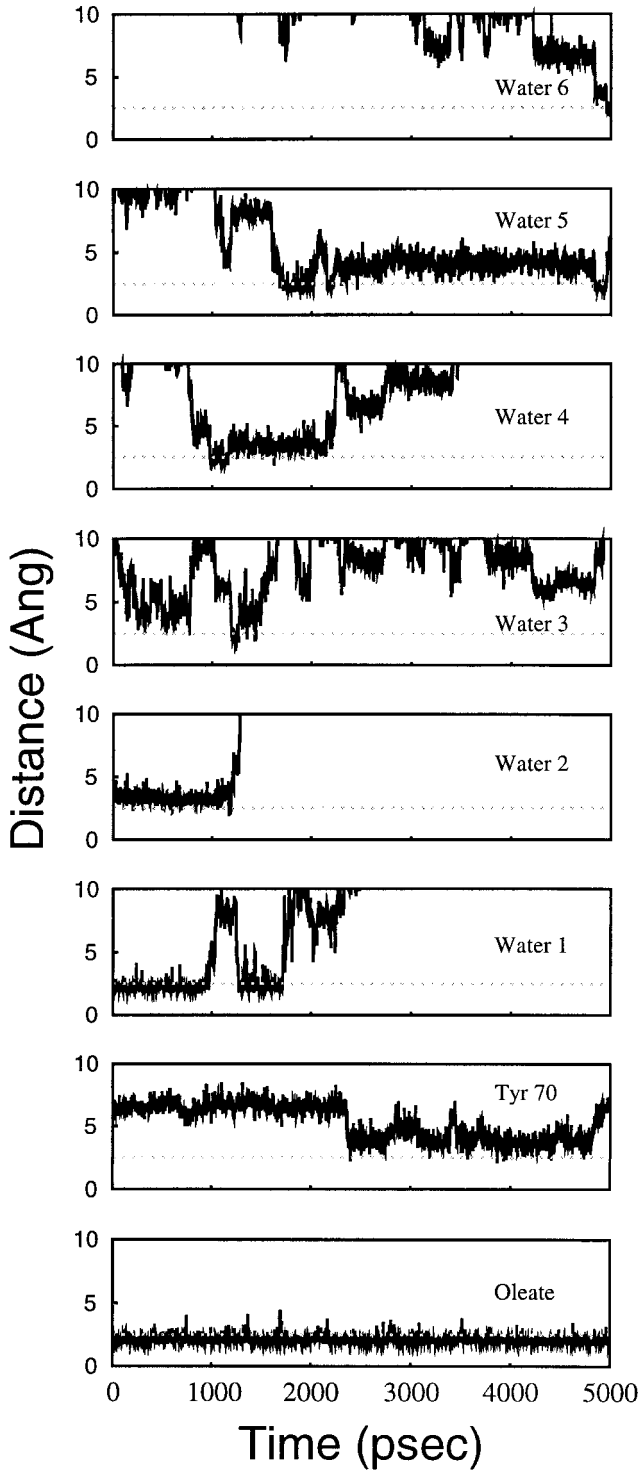

FIGURE 10 Trp-82 had different patterns of hydrogen bonding between apo and holo (oleate) simulations. The bottom panel shows that a tight hydrogen bond between the oleate and the ring hydrogen existed throughout the simulation. In the absence of the bond, the apo simulation had a population of 6 waters and a hydrogen bond from the ring oxygen of Tyr-70 that provided bonding during the simulation.

Thus, it was interesting to look for changes in the behavior of Phe55 in response to the different ligands and to contrast the behavior with that seen in the apo form. Analysis of the interaction energies shows that the strongest interactions to water were with the external water population (not shown). In this case the palmitate interaction was the weakest (near −10 kcal/mol), while the remaining three simulations showed interaction energies near −15 kcal/mol. The backbone-defined waters were the next strongest (−5 kcal/mol), the strictly defined internal waters the next (−4 kcal/mol; in Fig. 6), and the side chain waters the least strong interaction (−2 kcal/mol). The strongest interactions overall occurred with the backbone atoms of the protein (−33 kcal/mol), whereas the side chain interactions were less strong (−10 kcal/mol; in Fig. 6). Covariance analysis suggested relatively minor differences in coupling to the rest of the protein. The simulations suggest strong positive coupling to the immediate neighbors (S53, N54, R56, N57), and anticorrelated coupling to a set of residues that varied with apo/holo environment. The apo simulation showed strong anticorrelations to twelve sites (V25, V60, V61, V66, D67, F68, A69, L78, T79, G80, T81, F93) that were not anticorrelated in the myristate or palmitate runs. Three of the sites (A69, L78, T79) were also strongly anticorrelated in the oleate trajectory. Additionally, the palmitate run saw strong anticorrelation only with somewhat near neighbors (I58, D59), and the myristate strong anticorrelation was to three main other regions (W6, K27, R28, K29, N111, E112, L113, I127, F128, K129, K130). This certainly supports the finding that the coupling of protein:protein elements depends on the ligand type and presence. The covariance analysis to the water from the protein showed a strong difference between the apo and holo forms. The apo form had a relatively large set of residues coupled either positively or negatively into the F55 site (positively: A1, T5, K7, D9, E12, F17, K20, G22, I23, K27, L30, H33, D34, N35; negatively: W6, V8, R10, N11, N13, Y14, K16, M18, V25, R28, K29, G31). In contrast, the myristate had no strongly positively coupled and only one strongly negatively correlated site (D9), the palmitate had two positively correlated (A1, E12), and one anticorrelated (R10), the oleate had one positively coupled (G4) and four negatively coupled (Y14, K16, F17, G22). The covariance analysis of F55 to the ligand also showed differences between the holo runs. The palmitate coupling was positively coupled over the last nine heavy atoms and anticorrelated in coupling to the first half of the ligand. The myristate was anticorrelated only at four heavy atoms near the middle of the chain, and the oleate was anticorrelated at the carboxyl end, and in the later part of the middle, and positively correlated at other sites.

Thus, the suggestion that F55 regulates the length of the FABP binding site may be adjusted to suggest that the behavior of the side chain is sensitive to the presence of the ligand and couples in a different way to water, protein and ligand depending on the ligand type. In this regard it is also

worth noting that the χ-1 values of the apo, myristate, and oleate trajectories were roughly similar (averages of -61.6, -57.9, and -63.9 with rms fluctuations of 10.4, 9.4, and 10.4 respectively). In contrast, the palmitate χ-1 was -167.9 with fluctuations of 11.9, suggesting that the shifts in position may not be a simple linear shift in the χ-1 angle with fatty acid length as originally proposed.

Tyr70 and Tyr117

Tyr70 and Tyr117 are both near the ligand binding site, but differ in that Y117 is near the midpoint of the alkane chain and Y70 is near the headgroup. The largest interaction energies came, in both cases, from backbone connections between the residue and the rest of the protein (from -40 to -45 kcal/mol). The water interactions were less strong, with Y117 having the larger contribution to the strictly defined internal waters (-5.0 kcal/mol; see Fig. 6). The protein:protein covariance plots suggest differences in coupling to the rest of the protein between the two Tyr (not shown). For example, Y70 couples very strongly to the protein with binding of palmitate and oleate and is more weakly coupled for both the apo and myristate. As a contrast, Y117 is coupled most strongly to the rest of the protein with the presence of myristate, and weakly coupled for the apo and palmitate/oleate holo trajectories. Intriguing also is that the anticorrelated coupling to the rest of the protein is strongest for Y70 for the palmitate and oleate, while the Y117 is weakest anticorrelated for palmitate and oleate.

Further support of the changes in Y70 and Y117 with ligand presence and type is shown in the coupling to water, where Y70 has strong coupling to water for palmitate and oleate, with much weaker coupling for myristate and apo. Y117 shows the strongest coupling to water for myristate, with almost no coupling to water in the apo case and weak coupling for the palmitate and oleate. The coupling to the ligand itself is quite strong for Y70 in the palmitate and oleate cases. The analysis shows 14 of 18 (palmitate) and 16 of 20 (oleate) heavy atom covariances are of magnitude greater than 0.2 for these two cases. The coupling of Y70 is weaker for myristate with 4 of 16 heavy atoms greater than 0.2 in magnitude. As a contrast, Y117 had a much weaker coupling to the ligand, with the myristate having the strongest and the palmitate the weakest series of covariances. Also interesting is that Y70 was positively correlated with the ligand at the carboxyl and methyl ends and negatively coupled at the midpoint. A somewhat similar pattern was calculated for Y117, with a less strong magnitude of coupling.

Water behavior

Complex water behavior was observed in all four simulations. The water was a dynamic part of the structure, moving from the inside to the outside and participating in a range of hydrogen bonding interactions. Some of these interactions were relatively long-lived, whereas others had a fairly rapid exchange of water partners during the simulation. From the water properties detailed in Tables 2 and 3, certain other features may be emphasized. For example, Table 2 shows a general trend for those waters with a large number of contacts to inside side chains to have longer lifetimes inside the cavity than those with contacts mainly to the backbone. Also, the number of contacts to other waters, on average, was similar regardless of whether the other contacts were to protein backbone or side chain sites. It was found that in the populations of the most common interior waters (40 total), those in the last three-quarters of the set were able to exchange with the outside waters. The paths of exit were defined to be either the D:E gap or the cap defined by the two helices and the C:D and E:F loops. Table 3 shows the variation in the backbone binding sites in terms of lifetime and percent time occupied. This prompts the suggestion that the variation in lifetimes may be experimentally accessible via NMR methods (Cistola and Hall, 1995; Mesgarzadeh et al., 1998).

CONCLUSION

Detailed correlations in motion and interaction are described that vary depending on apo and holo form in four molecular dynamics simulations of intestinal fatty acid binding protein. Dynamic water exchange with the small population of interior waters that define the binding site was seen on the molecular dynamics time scale. This analysis suggests that binding thermodynamics depends not simply on ligand interactions with a small subset of protein atoms, but dynamically on the range of motions coupling the water, protein, and ligand.

Support from the National Institutes of Health (GM54782), the American Heart Association (grant-in-aid), the Bard Foundation, and the Department of Physiology is thankfully acknowledged. The computer resources of the Maui High Performance Computing Center were instrumental in the calculations. The simulations of this paper were largely completed by March of 1997 and described at the Biophysical Society meeting of that year.

Helpful comments by Horia Petrache and Jonathan Sachs are gratefully acknowledged.

REFERENCES

Åqvist, J., C. Medina, and J.-E. Samuelsson. 1994. A new method for predicting binding affinity in computer-aided drug design. *Prot. Eng.* 7:385.

Brooks, B. R., R. E. Bruccoleri, B. D. Olafson, D. J. States, S. Swaminathan, and M. Karplus. 1983. CHARMM: a program for macromolecular energy minimization and dynamics calculations. *J. Comp. Chem.* 4:187–217.

Brown, M. L., R. M. Venable, and R. W. Pastor. 1995. A method for characterizing transition concertedness from polymer dynamics computer simulations. *Biopolymers.* 35:31–46.

Brünger, A., III, C. L. Brooks, and M. Karplus. 1984. Stochastic boundary conditions for molecular dynamics simulations of ST2 water. *Chem. Phys. Lett.* 105:495–500.

Cistola, D. P., and K. B. Hall. 1995. Probing internal water molecules in proteins using two-dimensional 19F–1H NMR. *J. Biomol. NMR.* 5:415–419.

Cistola, D. P., J. C. Sacchettini, L. J. Banaszak, M. T. Walsh, and J. I. Gordon. 1989. Fatty acid interactions with rat intestinal and liver fatty acid-binding proteins expressed in Escherichia Coli: a comparative 13C NMR study. *J. Biol. Chem.* 264:2700–2710.

Cistola, D. P., J. C. Sacchettini, and J. I. Gordon. 1990. 13C NMR studies of fatty acid-protein interactions: comparison of homologous fatty acid-binding proteins produced in the intestinal epithelium. *Mol. Cell Biochem.* 98:101–110.

Dill, K. A. 1997. Additivity principles in biochemistry. *J. Biol. Chem.* 272:701–704.

Eads, J., J. C. Sacchettini, A. Kromminga, and J. I. Gordon. 1993. *Escherichia coli*-derived rat intestinal fatty acid binding protein with bound myristate at 1.5 Å resolution and I-FABP (Arg106-Gln) with bound oleate at 1.74 Å resolution. *J. Biol. Chem.* 268:26375–26385.

Frieden, C., N. Jiang, and D. P. Cistola. 1995. Intestinal fatty acid binding protein: Folding of fluorescein-modified proteins. *Biochemistry.* 34: 2724–2730.

Frolov, A., and F. Schroeder. 1997. Time-resolved fluorescence of intestinal and liver fatty acid binding proteins: role of fatty acyl CoA and fatty acid. *Biochemistry.* 36:505–517.

Gilson, M., K. A. Sharp, and B. Honig. 1988. Calculating the electrostatic potential of molecules in solution. *J. Comp. Chem.* 9:327–335.

Hodsdon, M. E., and D. P. Cistola, D. P. 1997a. Discrete backbone disorder in the nuclear magnetic resonance structure of apo intestinal fatty acid binding protein: implications for the mechanism of ligand entry. *Biochemistry.* 36:1450–1460.

Hodsdon, M. E., and D. P. Cistola. 1997b. Ligand binding alters the backbone mobility of intestinal fatty acid-binding protein as monitored by 15N NMR relaxation and 1H exchange. *Biochemistry.* 36: 2278–2290.

Hodsdon, M. E., J. J. Toner, and D. P. Cistola. 1995. 1H, 13C and 15N assignments and chemical shift-derived secondary structure of intestinal fatty acid-binding protein. *J. Biomol. NMR.* 6:198–210.

Hodsdon, M. E., J. W. Ponder, and D. P. Cistola, D. P. 1996. The NMR solution structure of intestinal fatty acid-binding protein complexed with palmitate: application of a novel distance geometry algorithm. *J. Mol. Biol.* 264:585–602.

Kim, K., D. P. Cistola, and C. Frieden. 1996. Intestinal fatty acid binding protein: The structure and stability of a helix-less variant. *Biochemistry.* 35:7553–7558.

Kirk, W. R., E. Kurian, and F. G. Prendergast. 1996. Characterization of the sources of protein-ligand affinity: 1-sulfonato-8-(1′) anilinonaphthalene binding to intestinal fatty acid binding protein. *Biophys. J.* 70: 69–83.

Kurian, E., W. R. Kirk, and F. G. Prendergast. 1996. Affinity of fatty acid for rat intestinal fatty acid binding protein: further examination. *Biochemistry.* 35:3865–3874.

LaLonde, J. M., D. A. Bernlohr, and L. J. Banaszak. 1994. The up-and-down Beta-barrel proteins. *FASEB J.* 8:1240–1247.

Lee, F. S., Z. T. Chu, M. B. Bolger, and A. Warshel. 1992. Calculations of antibody-antigen interactions: microscopic and semi-microscopic evaluation of the free energies of binding of phosphorylcholine analogs to McPC603. *Protein Eng.* 5:215–228.

Lipari, G., and A. Szabo. 1982. Model-free approach to the interpretation of nuclear magnetic resoance relaxation in macromolecules. I. Theory and range of validity. *J. Am. Chem. Soc.* 104:4546–4559.

Lucke, C., C. Ludwig, M. Rademacher, D. Fushman, J. C. Sacchettini, and H. Ruterjans. 1997. Conformational flexibility concurs with ligand binding in fatty acid binding proteins. The Third International Conference on Lipid-Binding Proteins Poster:26.

Mesgarzadeh, A., S. Pfeiffer, J. Engelke, D. Lassen, and H. Ruterjans. 1998. Bound water in apo and holo bovine heard fatty-acid-binding protein determined by heteronuclear NMR spectroscopy. *Eur. J. Biochem.* 251:781–786.

Richieri, G. V., R. T. Ogata, and A. M. Kleinfeld. 1992. A fluorescently labeled intestinal fatty acid binding protein: interactions with fatty acids and its use in monitoring free fatty acids. *J. Biol. Chem.* 267: 23495–23501.

Richieri, G. V., R. T. Ogata, and A. M. Kleinfeld. 1994. Equilibrium constants for the binding of fatty acids with fatty acid-binding proteins from adipocyte, intestine, heart, and liver measured with the fluorescent probe ADIFAB. *J. Biol. Chem.* 269:23918–23930.

Richieri, G. V., R. T. Ogata, and A. M. Kleinfeld. 1995. Thermodynamics of fatty acid binding to fatty acid binding proteins and fatty acid partition between water and membranes measured using the fluorescent probe ADIFAB. *J. Biol. Chem.* 270:15076–15084.

Richieri, G. V., R. T. Ogata, and A. M. Kleinfeld. 1996. Kinetics of fatty acid interactions with fatty acid binding proteins from adipocyte, heart, and intestine. *J. Biol. Chem.* 271:11291–11300.

Richieri, G. V., P. J. Low, R. T. Ogata, and A. M. Kleinfeld. 1997. Mutants of rat intestinal fatty acid binding protein illustrate the critical role played by enthalpy-entropy compensation in ligand binding. *J. Biol. Chem.* 272:16737–16740.

Richieri, G. V., P. J. Low, R. T. Ogata, and A. M. Kleinfeld. 1998. Thermodynamics of fatty acid binding to engineered mutants of the adipocyte and intestinal fatty acid-binding proteins. *J. Biol. Chem.* 273:7397–7405.

Sacchettini, J. C., and J. I. Gordon. 1993. Rat intestinal fatty acid binding protein: A model system for analyzing the forces that can bind fatty acids to proteins. *J. Biol. Chem.* 268:18399–18402.

Sacchettini, J. C., J. I. Gordon, and L. J. Banaszak. 1989. Crystal structure of rat intestinal fatty-acid-binding protein. *J. Mol. Biol.* 208:327–339.

Sacchettini, J. C., G. Scapin, D. Gopaul, and J. I. Gordon. 1992. Refinement of the structure of *Escherichia coli*-derived rat intestinal fatty acid binding protein with bound oleate to 1.75- Å resolution. *J. Biol. Chem.* 267:23534–23545.

Scapin, G., J. I. Gordon, and J. C. Sacchettini. 1992. Refinement of the structure of recombinant rat intestinal fatty acid binding apoprotein at 1.2-Å resolution. *J. Biol. Chem.* 267:4253–4269.

Schlenkrich, M., J. Brickmann, A. D. MacKerell, Jr., and M. Karplus. 1996. An empirical potential energy function for phospholipids: criteria for parameter optimization and applications. *In* Biological Membranes: A Molecular Perspective from Computation and Experiment. K. M. Merz, Jr., and B. Roux, eds. Birkhauser Press. 31–81.

Tjandra, N., S. E. Feller, R. W. Pastor, and A. Bax. 1995. Rotational diffusion anisotropy of human ubiquitin from 15N NMR relaxation. *J. Am. Chem. Soc.* 117:12562–12566.

Woolf, T. B. 1998. Simulations of fatty acid-binding proteins suggest sites important for function. I. Stearic acid. *Biophys. J.* 74:681–693.

Woolf, T. B., and M. Tychko. 1998. Simulations of fatty acid-binding proteins II: Sites for discrimination of monounsaturated ligands. *Biophys. J.* 74:694–707.

Wrabl, J., D. Shortle, and T. B. Woolf. 1998. Molecular dynamics simulations of native and denatured staphylococcal nuclease. *Biophys. J.* 74:A171.

Zhang, F., C. Lucke, L. J. Baier, J. C. Sacchettini, and J. A. Hamilton. 1997. Solution structure of human intestinal fatty acid binding protein: implications for ligand entry and exit. *J. Biomol. NMR.* 9:213–228.

Zhu, L., M. D. Kemple, E. Kurian, and F. G. Prendergast. 1997. Backbone dynamics of the rat intestinal fatty acid binding protein by 15N NMR. *Biophys. J.* 72:A107.